Journal of the Meteorological Society of Japan

EARLY ONLINE RELEASE

The DOI for this manuscript is
DOI:10.2151/jmsj.2024-001
J-STAGE Advance published date: September 19th, 2023
The final manuscript after publication will replace the preliminary version at the above DOI once it is available.

Dependence of the radiative-convective equilibrium structure of the lower atmosphere of Venus on the thermodynamic model

Yoshiyuki O. TAKAHASHI

Department of Planetology, Kobe University, Japan
Center for Planetary Science, Kobe University, Japan

and

Yoshi-Yuki HAYASHI

Department of Planetology, Kobe University, Japan
Center for Planetary Science, Kobe University, Japan

and

George L. HASHIMOTO

Department of Earth Sciences, Okayama University, Japan

and

Kiyoshi KURAMOTO

Department of Cosmosciences, Hokkaido University, Japan

and

Masaki ISHIWATARI

Department of Cosmosciences, Hokkaido University, Japan

and

Hiroki KASHIMURA

Department of Planetology, Kobe University, Japan
Center for Planetary Science, Kobe University, Japan

September 4, 2023

Corresponding author: Yoshiyuki O. Takahashi, Department of Planetology, Kobe University, 1-1, Rokkodaicho, Nada-ku, Kobe 657-8501, Japan.
E-mail: yot@gfd-dennou.org

Abstract

Dependence of the radiative-convective equilibrium structure of the lower atmosphere of Venus on the specification of atmospheric thermodynamic model is investigated. A series of thermodynamic models including ideal gases, van der Waals gases, and real gases are introduced by the use of the Helmholtz energy given by the EOS-CG mixture model (EOS-CG: Equation of State for Combustion Gases and Combustion Gas-like Mixtures). It is demonstrated that the radiative-convective equilibrium profile for the real gas differs significantly from that for the ideal gas with temperature-dependent specific heat by an increase of about 7 K in the surface temperature. This difference is caused by the fact that the adiabatic lapse rate evaluated with the thermodynamic model of real gas is larger than that of ideal gas, since the non-ideality of gas increases the thermal expansion coefficient, which overwhelms the increases of density and specific heat. It is confirmed that, in order to obtain better calculations of atmospheric circulations including the lower atmosphere of Venus, the ideal gas with a constant specific heat should be abandoned. The ideal gas with a temperature-dependent specific heat may not be enough. A promising method is to use the ideal gas but with the temperature-dependent specific heat such that its adiabatic lapse rate profile mimics that for the real gas.

Keywords Venus; one dimensional radiative-convective equilibrium state; non-ideal gas

1. Introduction

The surface environment of Venus is characterized by high pressure (∼92 bar) and high temperature (∼735 K) (e.g., Seiff et al. 1985), and the atmosphere at around the surface is in a supercritical state of CO_2. Elucidation of the lower atmosphere of Venus, the altitude region from the surface to the cloud layer at around 50 to 70 km, has not progressed very far, since it is difficult to observe the lower atmosphere which is shrouded by thick clouds.

Valuable data on the lower atmosphere of Venus were obtained by in situ observations by the Venera probes, the Pioneer Venus probes, and the VeGa-2 lander. Because of high temperature and high pressure in the lower atmosphere of Venus, the non-ideality of gas should be considered in estimating thermodynamic quantities, such as the adiabatic lapse rate, accurately (e.g., Staley 1970). In fact, in situ observational data were analyzed with considering the non-ideality of gas. The resultant analyses indicate that the atmosphere below the cloud layer is generally stable except for several altitude regions. (e.g., Seiff 1983).

Theoretical investigations, on the other hand, of the thermal structure of the Venus atmosphere have been carried out by the use of one-dimensional radiative-convective equilibrium models (Pollack and Young 1975; Matsuda and Matsuno 1978; Takagi et al. 2010; Ikeda 2011; Lee and Richardson 2011; Lebonnois et al. 2015; Mendonça et al. 2015). Those studies obtained possible thermal structures in radiative equilibrium and in radiative-convective equilibrium of the lower atmosphere. Some of those studies also addressed the dependence of the thickness of convection layers on the atmospheric composition and the cloud amount. Further, in recent years, numerical simulations by the use of three-dimensional general circulation models (GCMs) with explicit radiative transfer processes have been performed (e.g., Lebonnois et al. 2010; Ikeda 2011; Mendonça and Read 2016; Yamamoto et al. 2019). Among those studies, Lebonnois et al. (2018) investigated the structure of the planetary boundary layer in detail. Their model indicated that the thickness of the convective planetary boundary layer was less than 2 km varying diurnally and controlled by the radiative and the dynamical processes.

However, all of the above models with explicit model descriptions treat the Venusian atmosphere as an ideal gas. In addition, some of the circulation models mentioned above have been assuming that the specific heat is constant following the traditional formulation in Earth's meteorology. We believe that it is, in the first place, necessary to understand the effects of the non-ideality of the Venus atmospheric gas on the equation of state and the specific heat, since they are the key elements for the evaluation of static stability of the atmosphere. It is also important to recognize the deficits of assuming an ideal gas or a constant specific heat in considering the structure of the Venus atmosphere.

In this study, the thermal structure of the Venus atmosphere is investigated by the use of a one-dimensional radiative-convective equilibrium model with a series of thermodynamic models, i.e., ideal gases, van der Waals gases, and real gases given by specifying a thermodynamic potential such as Helmholtz energy or by specifying a set of equation of state (EOS) and specific heat. We focus on the dependence of the radiative-convective equilibrium structure of the lower atmosphere on the specification of atmospheric thermodynamic properties.

In the followings, in Section 2, the difference in static stability evaluated for a typical Venus atmospheric profile by the use of different thermodynamic models is discussed. Then, the one-dimensional radiative-convective equilibrium model for the Venus atmosphere utilized in this study is described in Section 3. The basic settings for the experiments are also described, there. In Section 4, the results of the radiative-convective equilibrium calculations are presented. The effects of non-ideality of gas are discussed, and the implications for dynamical calculations are presented in

Section 5. Finally, we conclude this study in Section 6.

2. Static stability of the VIRA model

Fig. 1

First, we evaluate the profiles of static stability for various thermodynamic models with the low latitude temperature profile of the VIRA (Venus International Reference Atmosphere) model (Fig. 1a) to give a picture of possible influence caused by the specification of thermodynamic properties.

We adopt the EOS-CG mixture model (Gernert and Span 2016) to evaluate the thermodynamic quantities of the Venus atmospheric gas. The EOS-CG mixture model describes the reduced Helmholtz energy of a mixture of real gases as sum of an ideal gas part and a residual part. The ideal gas part is expressed as the sum of the reduced Helmholtz energy of each component assumed as an ideal gas and a term accounting for the entropy of mixing. The residual part is expressed as the sum of the residual of the reduced Helmholtz energy of each component from an ideal gas and the departure function which is fitted to represent experimental thermodynamic properties for binary mixtures. Any thermodynamic quantities can be calculated directly from the reduced Helmholtz energy of the EOS-CG mixture model.

The use of the thermodynamic model requires much larger amount of computations than the use of the ideal gas law and a given specific heat.

For instance, the reduced Helmholtz energy of CO_2 described by Span and Wagner (1996), which is a component of the EOS-CG mixture model, is expressed as sum of 50 terms. Calculations of any thermodynamic quantities derived from the reduced Helmholtz energy require computations of larger number of terms. Further, an iterative procedure required to calculate density increases the amount of computation. The density has to be calculated, first, to calculate any thermodynamic quantities from the Helmholtz energy as functions of temperature and density by the use of the temperature profile as a function of pressure as an input. Such computations would be too expensive to be included in dynamical models, such as GCMs, but is acceptable in the data analysis and one-dimensional model calculations.

In our calculations of the thermodynamic properties, the atmospheric gas is assumed, unless otherwise mentioned, to be a mixture of CO_2 and N_2 gases with the volume mixing ratios of 0.965 and 0.035, respectively (von Zahn et al. 1983). Lebonnois and Schubert (2017) proposed that density-driven separation changes the mixing ratios of CO_2 and N_2 vertically and it could explain the temperature profile observed below 7 km altitude by the VeGa-2 lander (Seiff and the VEGA Balloon Science Team 1987). However, the details of the process in the Venus atmosphere have not been understood, and we do not investigate its effect on the thermal structure in the present study.

Figure 1b shows profiles of static stability, $dT/dz + gT\alpha_T/C_p$, evaluated with the EOS-CG mixture model (hereafter referred to as the real gas) and the EOS-CG mixture model but with the ideal gas part only (referred to as the ideal gas), where T, z, g, $\alpha_T = -(1/\rho)\left(\partial\rho/\partial T\right)_p$, ρ, and C_p, are temperature, the altitude, the gravitational acceleration set to 8.9 m s^{-2}, the thermal expansion coefficient, density, and the specific heat at constant pressure, respectively. In either case of the real gas or the ideal gas, an unstable (convective) layer at around 10^5 Pa pressure level and stable layers above and below it appear. In addition, layers close to neutral are also found just above the surface and at around 2×10^6 Pa pressure level in both profiles. However, details of stability differ between the two cases. The layer just above the surface is stable for the real gas, while it is unstable for the ideal gas. Further, the thickness of the unstable layer at around 2×10^6 Pa pressure level changes; the evaluation with the real gas tends to be more stable. Fig. 2

Also shown in Fig. 1b is the static stability profiles evaluated with the EOS of ideal gas but with constant C_p. The adopted values for C_p are 850 and 1150 J K^{-1} kg^{-1}, which correspond to the values at around 5×10^4 Pa pressure level where the temperature is about 300 K and 6×10^6 Pa pressure level where the temperature is about 680 K in the Venus atmosphere, respectively. It is found that the static stability profiles for the ideal gas but with constant C_p are quite different from those evaluated with the real gas or the ideal gas given by the EOS-CG mixture model. As for the static stability profile evaluated with $C_p = 850$ J K^{-1} kg^{-1}, the layers close to neutral below the cloud layer are not found anymore, although the static stability in the convective cloud layer is close to those evaluated with the EOS-CG mixture model. In addition, the static stability above the cloud layer differs as large as 20 % compared to those evaluated with the EOS-CG mixture model. As for the profile evaluated with $C_p = 1150$ J K^{-1} kg^{-1}, the static stability at around the surface is now close to those evaluated with the EOS-CG mixture model. However, the static stability above there is negative in several layers. If we adopt a smaller value, $C_p < 850$ J K^{-1} kg^{-1}, the static stability above the cloud layer can be closer to those evaluated with the EOS-CG mixture model, but then the static stability below the cloud layer must be the larger. These behaviors can be interpreted by examining the profiles of C_p. Figure 2 shows vertical profiles of C_p of the VIRA model, the real gas and the ideal gas for the low latitude temperature profile of the VIRA model. The corresponding profile calculated with $C_p(T) = C_{p0}(T/T_0)^{\nu}$ where $C_{p0} = 1000$ J kg^{-1} K^{-1}, $T_0 = 460$ K, and $\nu = 0.35$ used by Lebonnois et al. (2010) is also shown for reference. It is impossible to give an appropriate adiabatic lapse rate uniformly from the bottom to the top of the Venus atmosphere for the ideal gas but with constant C_p.

3. Model and experimental setup

The radiative-convective equilibrium solution is obtained as a steady state reached by time integration from a given initial condition. The dry convective adjustment is applied when the lapse rate is greater than the dry adiabatic lapse rate. In addition, surface temperature is assumed to be the same as atmospheric temperature just above the surface due to the convection.

Assuming the hydrostatic balance, the atmospheric energy equation for a stable layer is written as

$$C_p \frac{\partial T}{\partial t} = g \frac{\partial F_{rad}}{\partial p}, \tag{1}$$

and that for an unstable layer with the top pressure level p_t and the bottom pressure level p_b is written in an integrated form as

$$\int_{p_t}^{p_b} C_p \frac{\partial T}{\partial t} dp = \begin{cases} g(F_{rad}(p_b) - F_{rad}(p_t)) + gF_{sens}(p_s) & (\text{for} \quad p_b = p_s) \\ g(F_{rad}(p_b) - F_{rad}(p_t)) & (\text{for} \quad p_b < p_s) \end{cases} \tag{2}$$

with a vertical temperature gradient of

$$-\frac{dT}{dz} = \frac{g}{C_p} T \alpha_T, \tag{3}$$

where t, p, p_s, F_{rad}, and F_{sens} are time, pressure, the surface pressure, the net radiative flux, and the sensible heat flux, respectively. Note that upward fluxes are defined as positive.

The bottom surface is assumed to be a uniform slab. The energy equation for the surface slab is written as

$$C_s \frac{dT_s}{dt} = -F_{rad}(p_s) - F_{sens}(p_s), \tag{4}$$

where T_s and C_s are the surface temperature and the surface heat capacity arbitrarily set to 4.217×10^7 J K^{-1}, respectively. It is noted that the equilibrium solution is independent of the value of C_s.

Same as in Section 2, the atmospheric gas of Venus in our radiative-convective model is assumed to be, unless otherwise mentioned, a mixture of CO_2 and N_2 gases with the volume mixing ratios of 0.965 and 0.035, respectively, when evaluating the thermodynamic properties by the use of the EOS-CG mixture model.

The radiative fluxes are calculated by the use of the correlated k-distribution radiation model for Venus atmosphere of Takahashi et al. (2023). The radiative transfer equation with the generalized two-stream approximation (Meador and Weaver 1980) is solved with the method of Toon et al. (1989). In calculating radiative fluxes, absorption and scattering of molecular species and cloud particles are considered. Molecular species considered in radiation calculations are H_2O, CO_2, CO, SO_2, HF, OCS, and N_2.

It should be noticed that radiative fluxes are evaluated with considering species other than CO_2 and N_2, though the thermodynamic quantities are evaluated for the mixture of CO_2 and N_2. As for the cloud particles, those referred to as modes 1, 2, 2', and 3, whose particle sizes are different (Esposito et al. 1983; Ragent et al. 1985), are considered. In addition, "unknown UV absorber" which contributes almost the half of absorption of solar radiation (Crisp 1986) is also considered.

The vertical profiles of the radiatively active atmospheric components, the clouds, and the unknown UV absorber are externally given and fixed. Volume mixing ratios of radiatively active gases are based on Pollack et al. (1993) (Fig. 3a). As for the clouds and the unknown UV absorber, mass mixing ratios are based on Crisp (1986) (Fig. 3b). The profiles of radiatively active gases are those of Profile B of Takahashi et al. (2023), and the profiles of the clouds and the unknown UV absorber are the same as those of Takahashi et al. (2023).

The radiative-convective model is discretized with the 80 atmospheric layers (81 levels) determined by using those of the VIRA model as a reference. The thickness of each layer is 1 km from the surface to 60 km altitude and 2 km above. It has been confirmed that almost the same thermal structures are obtained when the number of layers are increased. A weak vertical filter is applied to avoid vertical two-grid interval noise only in some cases in which very shallow surface convection layers appear (Takahashi et al. 2023). The initial condition is the low latitude temperature profile of the VIRA model (Fig. 1a).

The incident solar radiation flux at the top of the atmosphere is assumed to be 2635 W m^{-2}. The surface albedo is set to 0.05 in wavenumber larger than 7700 cm^{-1}, and is zero in smaller wavenumber range. This is roughly consistent with the observations shown in Golovin et al. (1983). In order to evaluate the global mean of solar radiation, radiative fluxes are calculated at two solar zenith angles of 37.9° and 77.8°, and are averaged, and halved considering no contribution of nightside (Takahashi et al. 2023). Fig. 3

4. Results

4.1 Radiative-convective equilibrium structures

Fig. 4

Figure 4 shows the radiative-convective equilibrium profiles calculated for the real gas. The low latitude temperature and the static stability profiles of the VIRA model are also shown for comparison. The equilibrium is achieved by time integration for about 2×10^5 Earth days. The equilibrated surface temperature is 721 K. This is lower than 735 K observed by Venera 12 (Avduevskiy et al. 1983). The radiative-convective equilibrium profile represents the convective cloud layer at around 10^5 Pa pressure level and the stable layers below and above it as observed in the VIRA model. In the lower atmosphere, the surface convection layer is quite thick and its thickness is 34 km. This means that this radiative-convective equilibrium does not reproduce the observed stable layer at around 10–20 km altitude (e.g., Seiff 1983). The surface temperature lower than observed value and the lack of the stable layer at around 10–20 km altitude imply deficits of molecular and/or cloud particle opacities in the present model atmosphere, and also may be caused by the neglect of the horizontal variation in the one-dimensional model. It was discussed that the opacity in the 3–4 μm and 5–7 μm windows controls the surface temperature and atmospheric temperature in the deep atmosphere (cf. Lebonnois et al. 2015).

4.2 Dependence on thermodynamic model

Table 1

Fig. 5

In the previous subsection, the radiative-convective equilibrium profile is obtained for the real gas composed of 96.5 % CO_2 and 3.5 % N_2. Hereafter, the experiment with the real gas is referred to as Case RGMix. In this subsection, dependence of the radiative-convective equilibrium structure on the specification of atmospheric thermodynamic model is investigated by performing sensitivity experiments with simplified atmospheric thermodynamic models.

The performed experiments are summarized in Table 1. The simplified thermodynamic models introduced are of the pure CO_2 real gas (Case $RGCO_2$), of the mixture of van der Waals gases (Case VDWGMix), of the pure CO_2 van der Waals gas (Case $VDWGCO_2$), of the mixture of ideal gases (Case IGMix), and of the mixture of ideal gases with 850 J K^{-1} kg^{-1} as the value of constant C_p (Case IG850). In Cases VDWGMix, IGMix, and IG850, the mixture of gases is composed of 96.5 % CO_2 and 3.5 % N_2, the same as in Case RGMix. Table 2

In Case $RGCO_2$, the EOS-CG mixture model is used to derive the thermodynamic property for the pure CO_2 real gas. In Cases VDWGMix and $VDWGCO_2$, the following van der Waals EOS is used:

$$\left(p - \frac{a\rho^2}{\bar{M}^2}\right)\left(1 - \frac{b\rho}{\bar{M}}\right) = \rho RT, \tag{5}$$

where $R = R^*/\bar{M}$, and R^* and $\bar{M}$ are the universal gas constant and the mean molecular weight, respectively. The constants, a and b, for the EOSs of pure van der Waals gases are shown in Table 2. The constants for the mixture of van der Waals gases are calculated with van der Waals mixing rule, i.e., for the mixture of CO_2 ($i = 1$) and N_2 ($i = 2$), the constants, a and b, are written as

$$a = \sum_{i=1}^{2}\sum_{j=1}^{2} \chi_i \chi_j a_{ij}, \tag{6}$$

$$b = \sum_{i=1}^{2}\sum_{j=1}^{2} \chi_i \chi_j b_{ij}, \tag{7}$$

where χ_i is the volume mixing ratio of ith component, a_{ij} and b_{ij} $(i = j)$ are a and b of each pure component, respectively, and a_{ij} and b_{ij} $(i \neq j)$ are given as

$$a_{ij} = (a_i a_j)^{1/2}, \tag{8}$$

$$b_{ij} = (b_i + b_j)/2. \tag{9}$$

The specific heat at constant volume, C_v, for the van der Waals gas (Cases VDWGMix and VDWGCO_2) is given as that of the corresponding ideal gas derived from the EOS-CG mixture model but only with the ideal gas part, and the C_p is calculated with $C_p - C_v$ derived from the van der Waals EOS. In Case IGMix also, the EOS-CG mixture model but only with the ideal gas part is used to derive $C_p(T)$ for the mixture of ideal gases.

Figure 5 shows the results of the experiment. The radiative-convective equilibrium structures in the experiment other than Case IG850 are described, first. Even if the thermodynamic model is different, the gross features as seen from the static stability are similar to each other; there are the convective cloud layer, the stable layers above and below it, and the thick surface convection layer. The surface convection layer thicknesses are almost the same, and are 34, 35, 35, 35, and 35 km for Cases RGMix, RGCO_2, VDWGMix, VDWGCO_2, and IGMix, respectively. However, due to the difference in the adiabatic lapse rate in those cases, the surface temperature is different as large as 7 K between Cases RGMix and IGMix. It may be worth notifying that, either for the cases of the mixture of gases or the pure CO_2 cases, the temperature profile obtained for the van der Waals gas is close to that obtained for the corresponding real gas, respectively.

As for Case IG850, the thermal structure is quite different from those in the other cases. The lower atmosphere is strongly stratified, and the surface convection layer thickness is less than 1 km. It should be pointed out that the lowest level of the model is located at 1 km and the convection layer shallower than 1 km cannot be explicitly represented in the present model. Thermal structures for other values of constant C_p are shown in Appendix A for reference.

5. Discussion

5.1 Effects of non-ideality of gas on adiabatic lapse rate

Adiabatic lapse rate is the important quantity which explains the difference in radiative-convective equilibrium structures in the cases with different thermodynamic models. The adiabatic lapse rate is defined as Eq. (3). In the present study, the quantities are plotted in the log-pressure coordinate, the expression of the adiabatic lapse rate in the log-pressure coordinate is more useful:

$$\frac{dT}{d(lnp)} = \frac{p}{\rho C_p} T \alpha_T. \tag{10}$$

For an ideal gas, $\alpha_T = 1/T$, and the adiabatic lapse rate is $p/(\rho C_p)$. The difference in the adiabatic lapse rate between the real gas and the ideal gas for given p and T appears through differences in the density, the specific heat at constant pressure, and the thermal expansion coefficient. Conversely, the accurate value of $\alpha_T/(\rho C_p)$ is required for calculating the accurate radiative-convective equilibrium structure. Fig. 6

Fig. 7 Figure 6 shows relative differences of the density, the specific heat at constant pressure, the thermal expansion coefficient, and the adiabatic lapse rate of the real gas composed of 96.5 % CO_2 and 3.5 % N_2 from those of the ideal gas with the same component for the low latitude temperature profile as a function of pressure of the VIRA model. In Fig. 7, the profiles of the density, the specific heat at constant pressure, the thermal expansion coefficient, and the adiabatic lapse rate themselves are shown for reference. The non-ideality of gas increases and decreases the density as the altitude decreases, but increases monotonically both the specific heat at constant pressure and the thermal expansion coefficient. The magnitude of the increase in the thermal expansion coefficient is the largest among the changes in these three quantities. Consequently, the non-ideality of gas increases the adiabatic lapse rate, because it is inversely proportional to the density and the specific heat at constant pressure while proportional to the thermal expansion coefficient as seen in Eq. (10). The relative difference between the adiabatic lapse rate of the real gas and that of the ideal gas is as large as 4.5 % for the VIRA model profile.

5.2 Implications for dynamical models

In most of dynamical models, such as GCMs, for the Venus atmosphere, where fluid motions are explicitly calculated, the dynamical process is formulated with the assumption of ideal gas. Some of such models use the specific heat at constant pressure as a function of temperature. Lebonnois et al. (2010) formulated the governing equations with the assumption of ideal gas and with a temperature-dependent specific heat paying attention to a new expression of potential temperature, which is not too complex to be implemented in dynamical models. The use of the governing equations with the assumption of ideal gas is reasonable since the use of the thermodynamic model of real gas, such as the EOS-CG mixture model, is computationally expensive, and we have a rich heritage of the use of the model formulated with the assumption of ideal gas. In fact, as has been shown in previous sections, the use of the temperature-dependent specific heat with the assumption of ideal gas is much better than the use of a constant specific heat value.

However, the use of accurate temperature dependence of the specific heat at constant pressure only may not be enough to simulate the thermal structure of the real Venus atmosphere, since the effect of non-ideality especially in the thermal expansion coefficient cannot be ignored (Section 5.1).

Given a temperature profile as a function of pressure, the relative difference between the adiabatic lapse rate of the real gas, $dT/d(lnp) = pT\alpha_T/(\rho_{RG}C_{p,RG})$, and that of the ideal gas evaluated with C_p of the real gas, $dT/d(lnp) = p/(\rho_{IG}C_{p,RG})$, is $1 - (\rho_{RG}/\rho_{IG})/(T\alpha_T)$, where subscripts RG and IG stand for the real gas and the ideal gas, respectively. The relative difference is as large as 7.6 % for the VIRA model profile.

This is an amount which may not be neglected as an error. The malfunctions straightforwardly expected from the experience of the one-dimensional radiative-convective model are of the subgrid scale vertical mixing parameterizations, where the atmosphere is mixed vertically more or less when the lapse rate is smaller than the adiabatic lapse rate. The error in the evaluation of the adiabatic lapse rate influences the onset of the parameterizations and the value of the lapse rate after the mixing in the numerical model. Further, the same error affects not only the thermal structure of the atmosphere but also the dynamical structure. The error appears in the resolved adiabatic motions represented by the dynamical process. The value of the static stability or that of the adiabatic heating term in the temperature tendency equation is now different from the real Venus atmosphere, which affects the intensity of vertical winds, wave properties and so on. One may think that the adiabatic lapse rate of the real gas can be used for the critical value in the convective parameterizations. If such a method is adopted, then one should also change adiabatic heating term of the dynamical process consistently.

Another idea for possibly better dynamical calculations with the assumption of ideal gas is to set the temperature-dependent specific heat at constant pressure, $\tilde{C}_p$, such that the adiabatic lapse rate of the ideal gas, $p/(\rho_{IG}\tilde{C}_p)$, mimics the adiabatic lapse rate of the real gas, $pT\alpha_T/(\rho_{RG}C_{p,RG})$, for a typical profile. Then, the convection parameterizations mix the atmosphere with the adiabatic lapse rate corresponding to that of the real gas, and the adiabatic heating term in the dynamical process is also consistent with that of the real atmosphere. If we use the formulation of the governing equations of Lebonnois et al. (2010), the coefficients for the temperature-dependent specific heat at constant pressure, $C_p(T) = C_{p_0}(T/T_0)^\nu$, determined as suggested above for the low latitude temperature profile of the VIRA model are $C_{p_0} = 967$ J kg^{-1} K^{-1}, $T_0 = 460$ K, and $\nu = 0.30$. We have to note, however, that the temperature tendencies in the physical processes which depend on the specific heat, such as the radiative temperature tendency, have errors due to the difference from the specific heat for the real gas. The relative difference of these two values of the specific heat at constant pressure is $1 - (\rho_{RG}/\rho_{IG})/(T\alpha_T)$, and is the same as the relative difference in the adiabatic lapse rate described above.

6. Conclusions

The dependence of the thermal structure of the lower atmosphere of Venus on the specification of atmospheric thermodynamic model has been investigated. Static stability of the VIRA model profile has been evaluated by the use of the thermodynamic models with and without the assumption of ideal gas to examine the effects of non-ideality of gas. The layer just above the surface diagnosed as stable by the use of the thermodynamic model of the real gas is diagnosed as unstable by the use of the thermodynamic model of the ideal gas.

The radiative-convective equilibrium structure of the lower atmosphere of Venus has been investigated with various thermodynamic models. Between the cases with the real gas and the ideal gas the surface temperature differs as large as 7 K. If an ideal gas is assumed, the adiabatic lapse rate can deviate from that of the real gas by as much as 4.5 %. The deviation can be as much as 7.6 % if the specific heat at constant pressure of the real gas is used to evaluate the adiabatic lapse rate with the assumption of ideal gas. Since the layer of convection is determined by the adiabatic lapse rate, an inaccurate evaluation of the adiabatic lapse rate will significantly reduce the accuracy of the estimated thermal structure.

An idea to perform better dynamical calculations with the assumption of ideal gas is to use the specific heat at constant pressure such that the adiabatic lapse rate of the ideal gas mimics that of the real gas. In this approach, the convection parameterizations tend to mix the atmosphere vertically with the adiabatic lapse rate of the real Venus atmosphere. This procedure is consistent with the adiabatic heating in the dynamical processes, though the temperature tendencies of the physical processes which depend on the specific heat, such as radiative temperature tendency, are inaccurate.

Appendix A. Thermal structure in the cases with constant specific heat

Fig. 8

Figure 8 shows the radiative-convective equilibrium structures in the cases with the ideal gas but with the several values of constant specific heat at constant pressure, $C_p = 700, 850, 1000$, and 1150 J K^{-1} kg^{-1}.

Data Availability Statement

The data generated and analyzed in this study will be available at the JMSJ's J-STAGE Data site except for those already published elsewhere. Software developed and used in this study and its newest versions will be available from the web page of GFD Dennou Club, `https://www.gfd-dennou.org/`.

Acknowledgments

We are grateful to two anonymous reviewers for their constructive comments on this article. Visualization software developed by GFD Dennou Club, Dennou Club Library (DCL) and GPhys, are used to make plots shown in this study. A supercomputer of the Education Center on Computational Science and Engineering, Kobe University is used to perform several calculations shown in this study. This study was funded by Grant-in-Aid for Scientific Research on Innovative Areas (JSPS KAKENHI Grant Numbers 17H06457, 19H05605, and 21K03644) from Japan Society for the Promotion of Science.

References

Avduevskiy, V. S., M. Y. Marov, Y. N. Kulikov, V. P. Shari, A. Y. Gorbachevskiy, G. R. Uspenskiy, and Z. P. Cheremukhina, 1983: Structure and parameters of the Venus atmosphere according to Venera probe data. *Venus*, D. M. Hunten, L. Colin, T. M. Donahue and

V. I. Moroz, Eds., The University of Arizona Press, Tucson, Arizona chapter 12, 280–298.

Crisp, D., 1986: Radiative forcing of the Venus mesosphere I. Solar fluxes and heating rates. *Icarus*, **67**, 484–514.

Esposito, L. W., R. G. Knollenberg, M. Y. Marov, O. B. Toon, and R. P. Turco, 1983: The clouds and hazes of Venus. *Venus*, D. M. Hunten, L. Colin, T. M. Donahue and V. I. Moroz, Eds., The University of Arizona Press, Tucson, Arizona chapter 16, 484–564.

Gernert, J., and R. Span, 2016: EOS-CG: A Helmholtz energy mixture model for humid gases and CCS mixtures. *The Journal of Chemical Thermodynamics*, **93**, 274–293.

Golovin, Y. M., B. Y. Moshkin, and A. P. Ekonomov, 1983: Some optical properties of the Venus surface. *Venus*, D. M. Hunten, L. Colin, T. M. Donahue and V. I. Moroz, Eds., The University of Arizona Press, Tucson, Arizona chapter 7, 131–136.

Ikeda, K., 2011: *Development of radiative transfer model for Venus atmosphere and simulation of superrotation using a general circulation model*. PhD thesis, The University of Tokyo.

The Chemical Society of Japan, and H. Shinohara, 2004: *Handbook of Chemistry* (5 Ed.). Maruzen. (in Japanese)

Lebonnois, S., V. Eymet, C. Lee, and J. V. d'Ollone, 2015: Analysis of the radiative budget of the Venusian atmosphere based on infrared Net Exchange Rate formalism. *J. Geophys. Res.*, **120**, 1186–1200.

Lebonnois, S., F. Hourdin, V. Eymet, A. Crespin, R. Fournier, and F. Forget, 2010: Superrotation of Venus' atmosphere analyzed with a full general circulation model. *J. Geophys. Res.*, **115**, E06006.

Lebonnois, S., and G. Schubert, 2017: The deep atmosphere of Venus and the possible role of density-driven separation of CO_2 and N_2. *Nature Geoscience*, **10**, 473–477.

Lebonnois, S., G. Schubert, F. Forget, and A. Spiga, 2018: Planetary boundary layer and slope winds on Venus. *Icarus*, **314**, 149–158.

Lee, C., and M. I. Richardson, 2011: A discrete ordinate, multiple scattering, radiative transfer model of the Venus atmosphere from 0.1 to 260 μm. *J. Atmos. Sci.*, **68**, 1323–1339.

Matsuda, Y., and T. Matsuno, 1978: Radiative-convective equilibrium of the Venusian atmosphere. *J. Meteor. Soc. Japan*, **56**, 1–18.

Meador, W. E., and W. R. Weaver, 1980: Two-stream approximations to radiative transfer in planetary atmospheres: A unified description of existing methods and a new improvement. *J. Atmos. Sci.*, **37**, 630–643.

Mendonça, J. M., and P. L. Read, 2016: Exploring the venus global super-rotation using a comprehensive general circulation model. *Planet. Space Sci.*, **134**, 1–18.

Mendonça, J. M., P. L. Read, C. F. Wilson, and C. Lee, 2015: A new, fast and flexible radiative transfer method for Venus general circulation models. *Planet. Space Sci.*, **105**, 80–93.

Pollack, J. B., J. B. Dalton, D. Grinspoon, R. B. Wattson, R. Freedman, D. Crisp, D. A. Allen, B. Bezard, C. DeBergh, L. P. Giver, Q. Ma, and R. Tipping, 1993: Near-infrared light from Venus nightside: A spectroscopic analysis. *Icarus*, **103**, 1–42.

Pollack, J. B., and R. Young, 1975: Calculations of the radiative and dynamical state of the Venus atmosphere. *J. Atmos. Sci.*, **32**, 1025–1037.

Ragent, B., L. W. Esposito, M. G. Tomasko, M. Y. Marov, V. P. Shari, and V. N. Lebedev, 1985: Particulate matter in the Venus atmosphere. *Adv. Space Res.*, **5**, 85–115.

Seiff, A., 1983: Thermal structure of the atmosphere of Venus. *Venus*, D. M. Hunten, L. Colin, T. M. Donahue and V. I. Moroz, Eds., The University of Arizona Press, Tucson, Arizona chapter 11, 215–279.

Seiff, A., J. T. Schofield, A. J. Kliore, F. W. Taylor, S. S. Limaye, H. E. Revercomb, L. A. Sromovsky, V. V. Kerzhanovich, V. I. Moroz, and M. Y. Marov, 1985: Models of the structure of the atmosphere of Venus from the surface to 100 kilometers altitude. *Adv. Space Res.*, **5**, 3–58.

Seiff, A., and the VEGA Balloon Science Team, 1987: Further information on structure of the atmosphere of Venus derived from the VEGA Venus balloon and lander mission. *Adv. Space Res.*, **7**, 323–328.

Span, R., and W. Wagner, 1996: A new equation of state for carbon dioxide covering the fluid region from the triple-point temperature to 1100 k at pressures up to 800 mpa. *J. Phys. Chem. Ref. Data*, **25**, 1509–1596.

Staley, D. O., 1970: The adiabatic lapse rate in the venus atmosphere. *J. Atmos. Sci.*, **27**, 219–223.

Takagi, M., K. Suzuki, H. Sagawa, P. Baron, J. Mendrok, Y. Kasai, and Y. Matsuda, 2010: Influence of CO_2 line profiles on radiative and radiative‐convective equilibrium states of the venus lower atmosphere. *J. Geophys. Res.*, **115**, E06014.

Takahashi, Y. O., Y.-Y. Hayashi, G. L. Hashimoto, K. Kuramoto, and M. Ishiwatari, 2023: Development of a line-by-line and a correlated k-distribution radiation models for planetary atmospheres. *J. Meteor. Soc. Japan*, **101**, 2023–003.

Toon, O. B., C. P. McKay, T. P. Ackerman, and K. Santhanam, 1989: Rapid calculation of radiative heating rates and photodissociation rates in inhomogeneous multiple scattering atmospheres. *J. Geophys. Res.*, **94**, 16287–16301.

Yamamoto, M., K. Ikeda, M. Takahashi, and T. Horinouchi, 2019: Solar-locked and geographical atmospheric structures inferred from a Venus general circulation model with radiative transfer. *Icarus*, **321**, 232–250.

von Zahn, U., S. Kumar, H. Niemann, and R. Prinn, 1983: Composition of the Venus atmosphere. *Venus*, D. M. Hunten, L. Colin, T. M. Donahue and V. I. Moroz, Eds., The University of Arizona Press, Tucson, Arizona chapter 13, 299–430.

List of Figures

1 Vertical profiles of (a) temperature and (b) static stability for the VIRA model at low latitude. In panel (b), the red and the blue solid lines are for the real gas and the ideal gas, respectively, and the short-dashed and the dot-dashed blue lines are for the ideal gases with constant C_p of the values of 850 and 1150 J K^{-1} kg^{-1}, respectively. 31

2 Vertical profiles of specific heat at constant pressure for the low latitude temperature profile of the VIRA model. The black, the red, the blue, and the green lines show values of the VIRA model, the real gas, the ideal gas, and the temperature-dependent function used by Lebonnois et al. (2010), respectively. 32

3 Vertical profiles of gas volume mixing ratios and cloud mass mixing ratios used in the radiation model: (a) gas profile and (b) cloud profile. 33

4 Radiative-convective equilibrium (RCE) profiles of (a) temperature, (b) temperature difference from the low latitude profile of the VIRA model, and (c) static stability for the real gas (Case RGMix). 34

5 Radiative-convective equilibrium profiles of (a) temperature difference from the low latitude profile of the VIRA model, and (b) static stability with various thermodynamic models. The solid and the long-dashed red lines are those with Cases RGMix and $RGCO_2$, respectively. The solid and the long-dashed green lines are those with Cases VDWGMix and $VDWGCO_2$, respectively. The solid and the short-dashed blue lines are those with Cases IGMix and IG850, respectively. The black line is that for the low latitude profile of the VIRA model. 35

6 Relative differences of the density (solid), the specific heat at constant pressure (long-dashed), the thermal expansion coefficient (short-dashed), and the adiabatic lapse rate, $pT\alpha_T/(\rho C_p)$, (dot-dashed) of the mixture of real gases from those of the mixture of ideal gases for the low latitude temperature profile as a function of pressure of the VIRA model. 36

7 Vertical profiles of (a) the density, (b) the specific heat at constant pressure, (c) the thermal expansion coefficient, and (d) the adiabatic lapse rate of the mixture of real gases (red) and those of the mixture of ideal gases (blue) for the low latitude temperature profile as a function of pressure of the VIRA model. 37

8 Same as Fig. 4, but with the ideal gas with constant specific heat. The red, the green, the blue, and the magenta lines are the profiles for $C_p = 700, 850, 1000, 1150$ J K^{-1} kg^{-1}, respectively. 38

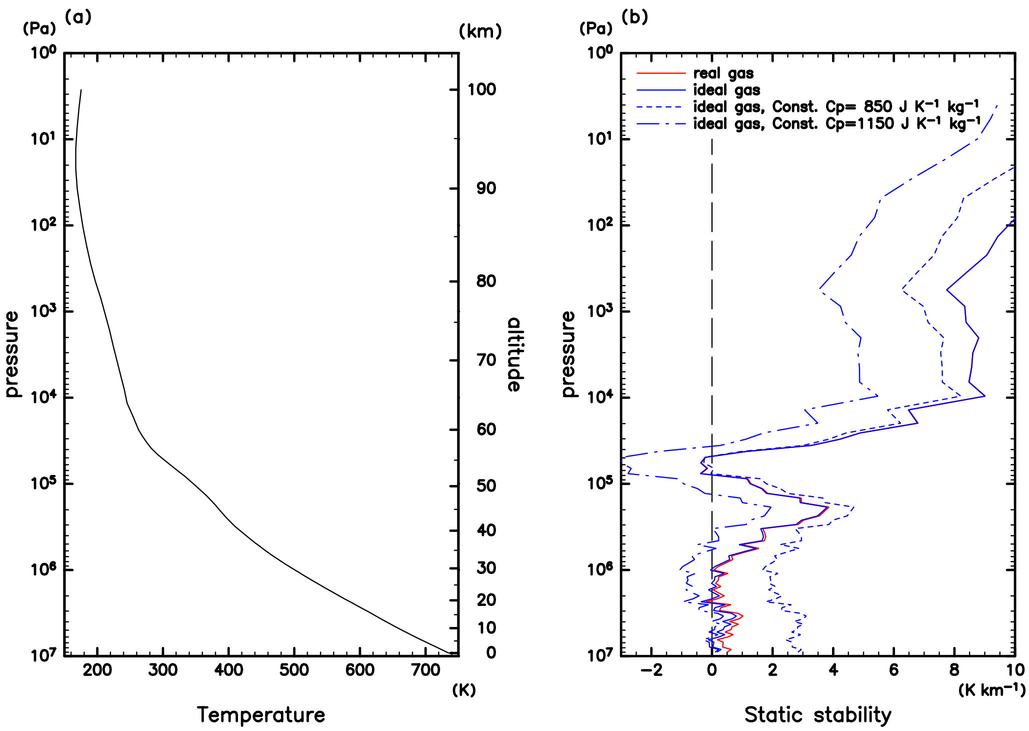

Fig. 1. Vertical profiles of (a) temperature and (b) static stability for the VIRA model at low latitude. In panel (b), the red and the blue solid lines are for the real gas and the ideal gas, respectively, and the short-dashed and the dot-dashed blue lines are for the ideal gases with constant C_p of the values of 850 and 1150 J K^{-1} kg^{-1}, respectively.

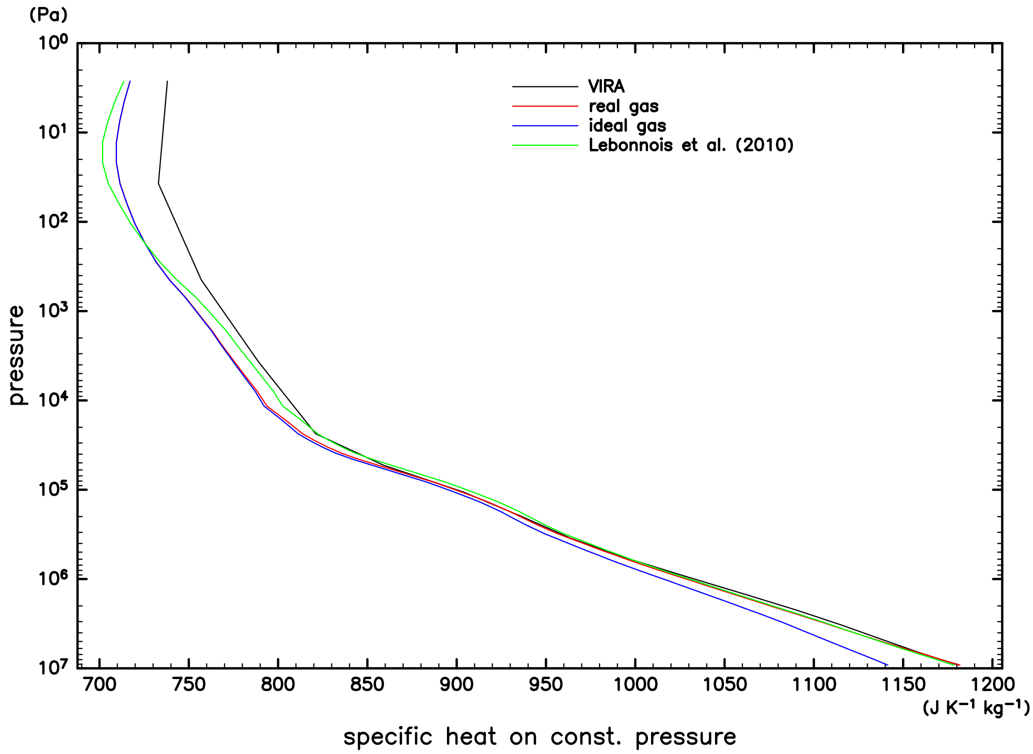

Fig. 2. Vertical profiles of specific heat at constant pressure for the low latitude temperature profile of the VIRA model. The black, the red, the blue, and the green lines show values of the VIRA model, the real gas, the ideal gas, and the temperature-dependent function used by Lebonnois et al. (2010), respectively.

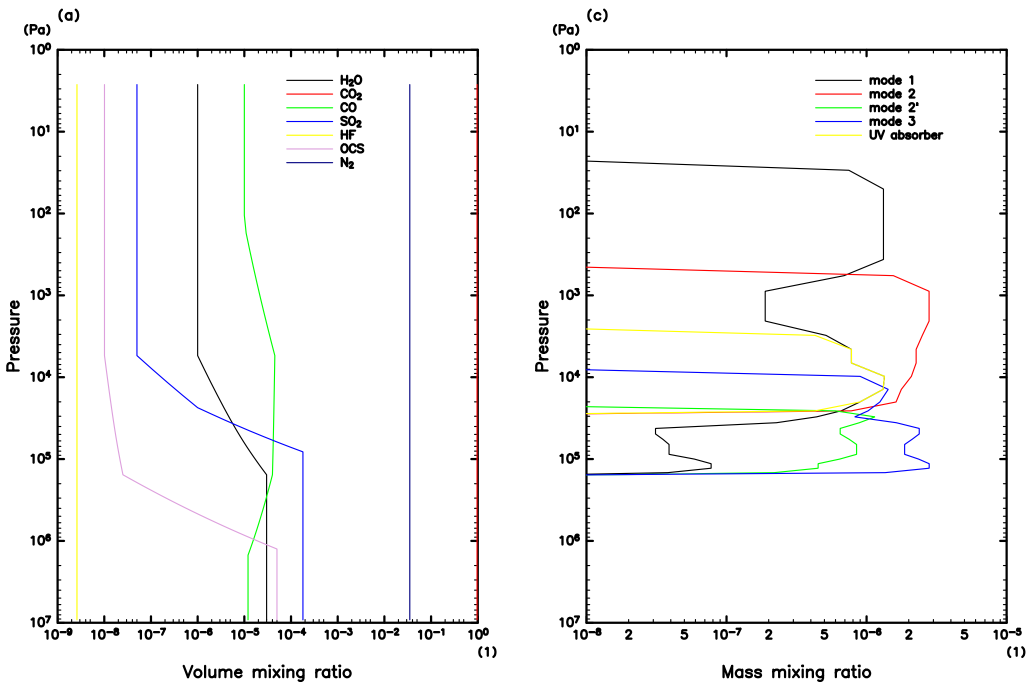

Fig. 3. Vertical profiles of gas volume mixing ratios and cloud mass mixing ratios used in the radiation model: (a) gas profile and (b) cloud profile.

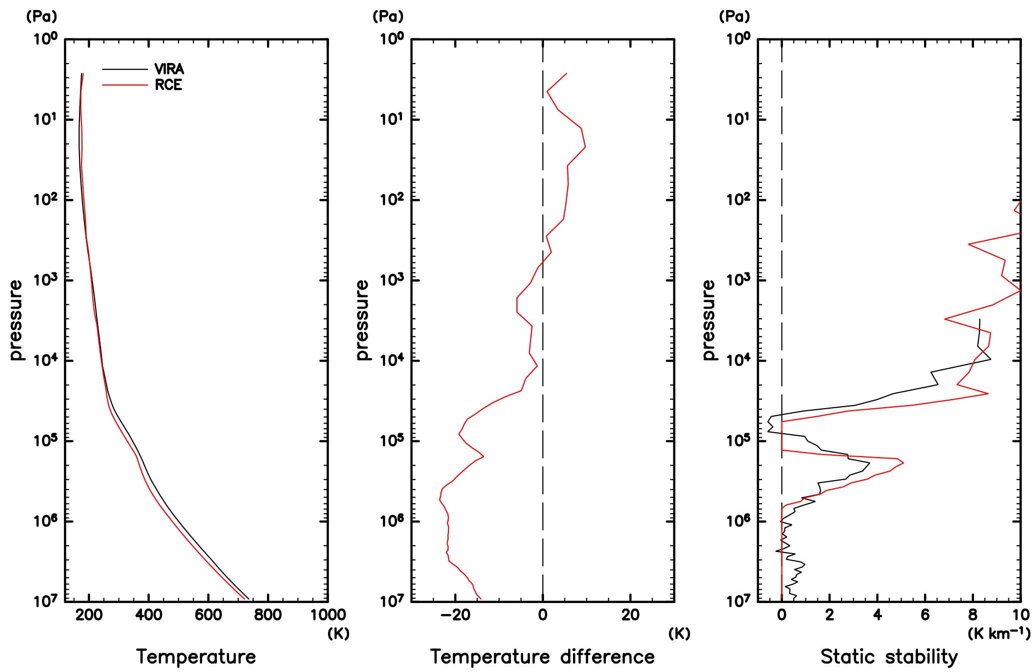

Fig. 4. Radiative-convective equilibrium (RCE) profiles of (a) temperature, (b) temperature difference from the low latitude profile of the VIRA model, and (c) static stability for the real gas (Case RGMix).

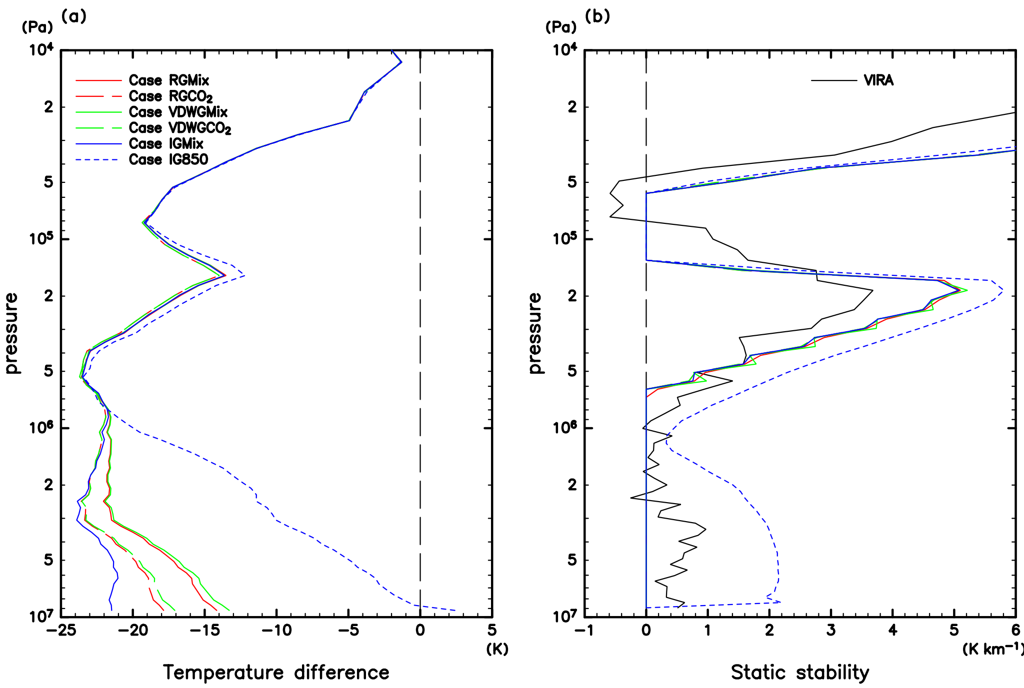

Fig. 5. Radiative-convective equilibrium profiles of (a) temperature difference from the low latitude profile of the VIRA model, and (b) static stability with various thermodynamic models. The solid and the long-dashed red lines are those with Cases RGMix and $RGCO_2$, respectively. The solid and the long-dashed green lines are those with Cases VDWGMix and $VDWGCO_2$, respectively. The solid and the short-dashed blue lines are those with Cases IGMix and IG850, respectively. The black line is that for the low latitude profile of the VIRA model.

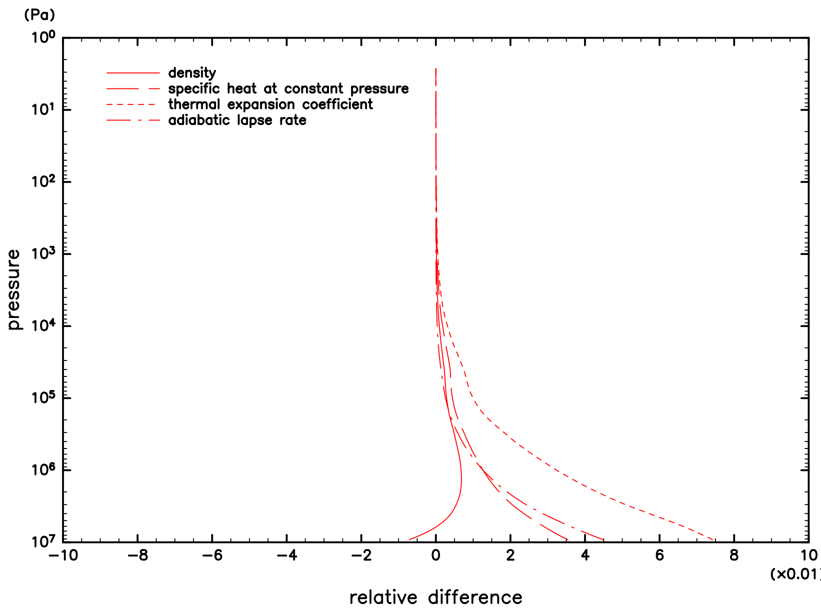

Fig. 6. Relative differences of the density (solid), the specific heat at constant pressure (long-dashed), the thermal expansion coefficient (short-dashed), and the adiabatic lapse rate, $pT\alpha_T/(\rho C_p)$, (dot-dashed) of the mixture of real gases from those of the mixture of ideal gases for the low latitude temperature profile as a function of pressure of the VIRA model.

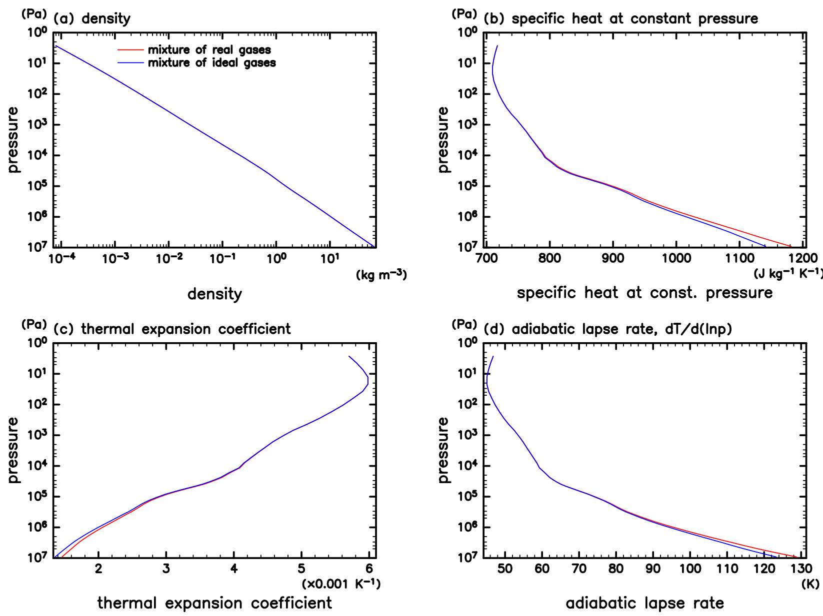

Fig. 7. Vertical profiles of (a) the density, (b) the specific heat at constant pressure, (c) the thermal expansion coefficient, and (d) the adiabatic lapse rate of the mixture of real gases (red) and those of the mixture of ideal gases (blue) for the low latitude temperature profile as a function of pressure of the VIRA model.

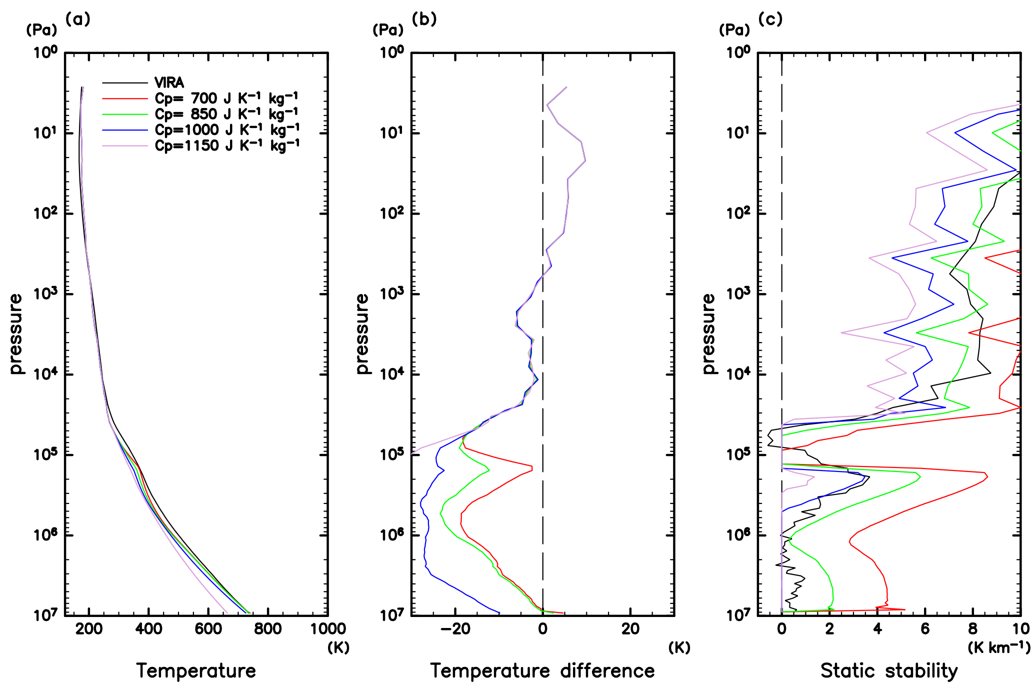

Fig. 8. Same as Fig. 4, but with the ideal gas with constant specific heat. The red, the green, the blue, and the magenta lines are the profiles for $C_p = 700, 850, 1000, 1150$ J K^{-1} kg^{-1}, respectively.

List of Tables

1 Thermodynamic models used in the experiments. 40
2 The constants, a and b, for van der Waals EOS for each pure component (The Chemical Society of Japan and Shinohara 2004). 41

Table 1. Thermodynamic models used in the experiments.

Case	EOS	C_p
RGMix	real gas EOS [a]	dependent on T and ρ [b]
$RGCO_2$	real gas EOS [a]	dependent on T and ρ [b]
VDWGMix	van der Waals EOS	dependent on T and ρ [c]
$VDWGCO_2$	van der Waals EOS	dependent on T and ρ [c]
IGMix	ideal gas EOS	dependent on T [b]
IG850	ideal gas EOS	850 J K^{-1} kg^{-1}

[a]The EOS-CG mixture model is used.
[b]The values are derived from the EOS-CG mixture model.
[c]The values are represented as the sum of C_v of ideal gases derived from the EOS-CG mixture model and $C_p - C_v$ derived from the van der Waals EOS.

Table 2. The constants, a and b, for van der Waals EOS for each pure component (The Chemical Society of Japan and Shinohara 2004).

Component	a (Pa m^6 mol^{-2})	b (m^3 mol^{-1})
CO_2	3.66×10^{-1}	4.28×10^{-5}
N_2	1.37×10^{-1}	3.36×10^{-5}